Soft Matter

Adsorption and aggregation properties of quaternary-ammonium-salt-based gemini surfactants with a glycinate counterion

Journal:	*Soft Matter*
Manuscript ID	SM-ART-02-2025-000139.R1
Article Type:	Paper
Date Submitted by the Author:	23-Mar-2025
Complete List of Authors:	Wang, Shan; Nara Women's University Iwase, Hiroki; Comprehensive Research Organisation for Science and Society, Research Center for Neutron Science & Technology Takata, Shinichi; J-Park Center, Materials & Life Science Facility Division Kawai, Risa; Nara Women's University Yada, Shiho; Tokyo University of Science - Katsushika Campus, Department of Industrial Chemistry, Faculty of Engineering Yoshimura, Tomokazu; Nara Women's University

ARTICLE

Adsorption and aggregation properties of quaternary-ammonium-salt-based gemini surfactants with a glycinate counterion†

Received 00th January 20xx,
Accepted 00th January 20xx

DOI: 10.1039/x0xx00000x

Shan Wang,[a] Hiroki Iwase,[b] Shin-ichi Takata,[c] Risa Kawai,[a] Shiho Yada [d] and Tomokazu Yoshimura *[a]

Cationic gemini surfactants have promising bioapplications that are limited by the use of halides as counterions, which pose environmental and human health risks. This can be circumvented by using naturally occurring, highly water-soluble, and nontoxic counterions such as amino acids. In this study, we synthesized novel quaternary-ammonium-salt-based cationic gemini surfactants with glycinate as the counterion [2C$_n$(2-O-2) Gly, where n is the alkyl chain length, n = 10, 12, 14]. Their adsorption and aggregation properties were investigated by measuring their electrical conductivity, surface tension, and small-angle neutron scattering and compared with those of the corresponding gemini surfactants with a bromide counterion [2C$_n$(2-O-2) Br]. The relationship between the surface tension and concentration of 2C$_n$(2-O-2) Gly exhibited a unique behavior with a pronounced minimum near the critical micelle concentration. This suggests that 2C$_n$(2-O-2) Gly adsorbs densely at the air/water interface through hydrogen bonding between the amino nitrogen of the counterion and hydrogen atoms of water, as well as between the carboxylate oxygen of the counterion and hydrogen atoms of either the amino group or water. In an aqueous solution, 2C$_n$(2-O-2) Gly formed small micelles, whose structure transitioned from spherical to ellipsoidal as the concentration increased.

Introduction

Gemini surfactants with two alkyl chains and two hydrophilic groups exhibit excellent surface activities such as high water solubility, low critical micelle concentration (CMC), and high efficiency in surface tension reduction compared with conventional monomeric surfactants.[1–3] Moreover, they exhibit unique aggregation behavior, such as spontaneous vesicle formation at low concentrations near the CMC in aqueous solutions. Whereas the adsorption and aggregation properties of conventional monomeric surfactants are affected by factors such as the structures of hydrophilic and hydrophobic groups, those of gemini surfactants are additionally influenced by the structure of the spacer group. The physicochemical properties of gemini surfactants, such as the CMC and surface tension, can be modulated by replacing hydrogen atoms in the hydrophobic groups with fluorine atoms,[4–7] incorporating hydrophilic groups with different structures,[8–11] and modifying the spacer structure.[12–15] For ionic surfactants, the CMC,[16–24] Krafft temperature (T_K),[25] and size and shape of micelles formed in aqueous solutions[26,27] depend on the structure of the counterion. Thomas et al. reported that the CMC of quaternary-ammonium-salt-based cationic gemini surfactants is related to the hydration radius, polarizability, and charge of the counterion and decreases in the order $F^- > Cl^- > CH_3COO^- > Br^- > NO^{3-} > SO_4^{2-}$.[28]

We previously demonstrated that quaternary-ammonium-salt-based cationic gemini surfactants with a fluorine-containing counterion, such as bis(trifluoromethanesulfonyl)imide [$(CF_3SO_2)_2N^-$], bis(fluorosulfonyl)imide [$(FSO_2)_2N^-$], and hexafluorophosphate (PF_6^-), exhibit significantly lower melting points and function as amphiphilic ionic liquids.[29,30] However, the presence of fluorine decreases water solubility, which prevents micelle formation in aqueous solutions. In addition to their low water solubility, such surfactants do not easily degrade in nature. Consequently, their concentrations in rivers and groundwater exceed water quality standards, raising concerns about their impact on the ecosystem owing to bioaccumulation. Furthermore, quaternary-ammonium-salt-based cationic surfactants commonly used in fabric softeners, hair rinses, and disinfectants have a halide counterion. The use of halide ions in drug delivery systems and food products has been restricted because they can potentially form carcinogenic and mutagenic halogenated compounds.

The environmental and human health risks posed by quaternary-ammonium-salt-based gemini surfactants can be mitigated by using naturally occurring counterions that are highly water soluble and harmless to the environment and human body. In this respect, amino acids, which are the constituents of proteins and essential for the maintenance of life, are ideal candidates for counterions. Amino acids have been used in various functional materials because they are safe for the environment and humans. Imidazolium-based cationic surfactants with an amino acid as the counterion have been developed.[31–33] Their CMC decreases in order Br^- > prolinate (Pro^-) > alaninate (Ala^-) > phenylalaninate (Phe^-).[31] However, quaternary-ammonium-salt-based surfactants with an amino acid counterion, including gemini ones, have not been reported.

In this study, we synthesized novel quaternary-ammonium-salt-based gemini surfactants with glycinate as the counterion [2C$_n$(2-O-2) Gly, where n is the alkyl chain length, n = 10, 12 and 14, Fig. 1]. Additionally, the effects of the counterion structure, alkyl chain length, and surfactant concentration on their adsorption and aggregation properties were investigated.

[a] Department of Chemistry, Faculty of Science, Nara Women's University, Kitauoyanishi-machi, Nara 630-8506, Japan. E-mail: yoshimura@cc.nara-wu.ac.jp
[b] Neutron Science and Technology Center, Comprehensive Research Organization for Science and Society (CROSS), Tokai, Ibaraki 319-1106, Japan
[c] Japan Proton Accelerator Research Complex (J-PARC), Japan Atomic Energy Agency, Tokai, Ibaraki 319-1195, Japan
[d] Department of Industrial Chemistry, Faculty of Engineering, Tokyo University of Science, 6-3-1 Niijuku, Katsushika-ku, Tokyo 125-8585, Japan
† Supplementary Information available: Additional experimental data, including synthesis routes; ^{1}H NMR spectra; elemental analysis; surface tension measurements; and scattering profiles. See DOI: 10.1039/x0xx00000x

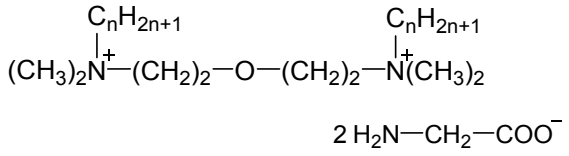

Fig. 1 Structure of $2C_n$(2-O-2) Gly (n = 10, 12, and 14).

Materials and methods

Materials

Bis(2-dimethylaminoethyl)ether, *n*-decyl bromide, *n*-dodecyl bromide, and *n*-tetradecyl bromide were purchased from Tokyo Chemical Industry Co., Ltd. (Tokyo, Japan). Glycine, acetonitrile, ethyl acetate, hexane, methanol, and 2-propanol were purchased from FUJIFILM Wako Pure Chemical Co., Ltd. (Osaka, Japan). The anion exchange resin (IRA402BL OH HG) was purchased from Organo Corporation (Tokyo, Japan). Deuterated chloroform and deuterated dimethyl sulfoxide used in the ^{1}H nuclear magnetic resonance (NMR) measurements were purchased from Cambridge Isotope Laboratories, Inc. (Andover, MA, USA). All chemicals were used without further purification. Ultrapure water (resistivity = 18.2 MΩ cm) from a Merck KGaA Direct-Q UV system (Darmstadt, Germany) was used in all the experiments.

Synthesis of bis[2-(*N*-alkyl-*N*,*N*-dimethylammonio)ethyl]ether bromide

n-Decyl bromide, *n*-dodecyl bromide, or *n*-tetradecyl bromide (2.2 equiv) was added dropwise to a heated solution of bis(2-dimethylaminoethyl)ether (10 g, 1.0 equiv) in an acetonitrile/2-propanol mixture (3:1, vol/vol), and the resulting mixture was stirred. After heating the mixture under reflux for 45 h, the solvent was evaporated under reduced pressure, and the residue was washed several times with hexane and ethyl acetate. The product was then recrystallized from an ethyl acetate/methanol mixture (3:2, vol/vol). Finally, the residue was dried under reduced pressure to obtain the quaternary-ammonium-salt-based gemini surfactant with a Br^- counterion, bis[2-(*N*-alkyl-*N*,*N*-dimethylammonio)ethyl]ether dibromide [$2C_n$(2-O-2) Br], as a white solid. The synthesis route is shown in Scheme S1.

Ion-exchange of Br^- in $2C_n$(2-O-2) Br with glycinate

A bis[2-(*N*-alkyl-*N*,*N*-dimethylammonio)ethyl]ether hydroxide [$2C_n$(2-O-2) OH] aqueous solution was prepared from $2C_n$(2-O-2) Br using an anion exchange resin and added dropwise to a slightly excess equimolar glycine aqueous solution. The mixture was stirred while cooling for 4 h. Subsequently, water was removed by freeze-drying for 2 d. An acetonitrile/methanol mixture (9:1, vol/vol) was added, and the mixture was stirred vigorously. The mixture was then filtered to remove excess glycine, and the filtrate was evaporated to remove the solvents. The product was dried in vacuo for 2 d at 45 °C. The structures of the resulting quaternary-ammonium-salt-based gemini surfactants with a glycinate counterion ($NH_2CH_2COO^-$), bis[2-(*N*-alkyl-*N*,*N*-dimethylammonio)ethyl]ether diglycinate [$2C_n$(2-O-2) Gly], were confirmed by ^{1}H NMR spectroscopy (JEOL JNM AL-400) and elemental analysis (Supplementary Information). The synthesis route is shown in Scheme S1.

Measurements

$2C_n$(2-O-2) Gly solutions were prepared using Milli-Q Plus water (resistivity = 18.2 MΩ cm), and measurements were performed at 25.0 ± 0.5 °C.

General properties

The electrical conductivity of each gemini surfactant in an aqueous solution was measured using a DKK-TOA CM-30R electrical conductivity meter (Tokyo, Japan) to determine the CMC. To ensure reproducibility, measurements were conducted three times for each surfactant concentration. The measurement uncertainties were within ± 0.3 mS m^{-1}, which was considered negligible. Therefore, error bars were not included in the conductivity plots. Surface tension was measured using a Krüss K122 tensiometer (Hamburg, Germany) by applying the Wilhelmy plate method. To ensure reproducibility, measurements were conducted at least five times for each surfactant concentration. The obtained values were used to construct the surface tension curves, and measurement uncertainties were evaluated and represented by error bars in the curves. The surface excess concentration (Γ, mol m^{-2}) and occupied area per molecule (A, nm^2 per molecule) at the air/water interface were calculated using the Gibbs adsorption isotherm equation $\Gamma = -(1/iRT)(d\gamma/d\ln C)$ and $A = 1/(N_A\Gamma)$, where γ is the surface tension, C is the surfactant concentration in the aqueous solution, R is the gas constant (8.31 J K^{-1} mol^{-1}), T is the absolute temperature, and N_A is Avogadro's constant. The value of i, which is the number of ionic species completely dissociated in the aqueous solution, was set to 3.

Small-angle neutron scattering (SANS)

SANS measurements were carried out using the small- and wide-angle neutron scattering instrument (TAIKAN) installed in the Material and Life Science Experimental Facility of the Japan Proton Accelerator Research Complex (J-PARC), Tokai, Japan.[34] Using large area detectors and white neutrons with a wavelength range of 0.08–0.78 nm, TAIKAN can simultaneously cover a scattering vector (q) range of 0.05–170 nm^{-1}. q is defined as $q = 4\pi\sin(\vartheta/2)/\lambda$, where ϑ and λ are the scattering angle and wavelength, respectively. In this study, the q range was limited to $0.1 < q < 5$ nm^{-1} because of instrumental background at $q < 0.1$ nm^{-1} and incoherent scattering from hydrogen atoms at $q > 5$ nm^{-1}. The sample temperature was maintained at approximately 25 °C by circulating water. Time-of-flight spectra were corrected for factors such as incident neutron distribution, detector efficiency, transmission, and background scattering. The scattering intensity $I(q)$ was then converted to the absolute intensity per sample volume by using a secondary standard of glassy carbon.[35] The solution was

enclosed in a quartz cell with a path length of 2 mm. The gemini surfactant solutions for SANS measurements were prepared using deuterium oxide (D_2O).

SANS model fitting analysis

Model fitting analysis of the SANS profiles was performed to investigate the structures and sizes of the micelles formed by the gemini surfactants in the aqueous solution. The $I(q)$ in the SANS profile of a micelle solution can be expressed by multiplying the form factor $P(q)$ by the structure factor $S(q)$ as follows:[36–38]

$$I(q) = N_P(\Delta\rho)^2 V_p{}^2 P(q) S(q) + I_{inc} \quad (1)$$

where N_P, $\Delta\rho$, and V_p are the number of particles, scattering contrast, and volume of a single particle, respectively. $\Delta\rho$ is defined as the difference between the scattering length densities of the gemini surfactant micelles and D_2O. I_{inc} is the incoherent scattering intensity (constant value). Considering previous SANS studies,[39–41] we employed the scattering function of a charged homogeneous prolate ellipsoid model. Here, the $P(q)$ of a homogeneous prolate ellipsoid with radius R is given by

$$P(q) = 9\int_0^1 \left[\frac{j_1(qR)}{qR}\right]^2 d\mu \quad (2)$$

where $j_1(x)$ is the first-order spherical Bessel function of x. R is defined as

$$R = \left[R_1{}^2\mu^2 + R_2{}^2(1-\mu^2)\right]^{1/2} \quad (3)$$

where μ is the cosine of the angle between vector q and the direction of major axis of the prolate model. The axial ratio v of the ellipsoidal micelles was calculated by dividing the radius of the major axis R_1 by the radius of the minor axis R_2. When surfactants form spherical micelles in an aqueous solution, the value of v is 1.

The interparticle structure factor $S_{HP}(q)$ for a charged micelle system interacting through a repulsive screened Coulomb potential is calculated using the rescaled mean spherical approximation as follows:[42,43]

$$S_{HP}(q) = \frac{1}{1-24\phi a(q\sigma)} \quad (4)$$

where φ is the volume fraction and σ is the effective particle diameter. $a(q\sigma)$, as defined by Hayter and Penfold,[42] depends on φ and the degree of ionization and corresponds to the Debye length l_d, which is given by

$$l_d = \left(\frac{\varepsilon\varepsilon_0 kT}{2N_A e^2 I}\right) \quad (5)$$

where ε is the dielectric constant of the solvent, ε_0 is the permittivity of free space, e is the electronic charge, and I is the ionic strength of the solution. For asymmetric particles such as ellipsoidal particles, the structure factor $S'(q)$ used for model fitting analysis is modified to account for anisotropy as follows:[44]

$$S'(q) = 1 + \frac{|\langle F(q)\rangle|^2}{\langle |F(q)|\rangle^2}(S_{HP}(q)-1) \quad (6)$$

where $F(q)$ is the scattering amplitude of the particle.

Results and discussion

Krafft temperature (T_K)

Clear 1.0 wt% aqueous solutions of gemini surfactants with a glycinate counterion [$2C_n$(2-O-2) Gly, n = 10, 12, and 14] were prepared and refrigerated at ~5 °C for at least 24 h. The solutions remained clear with no visible precipitates. Therefore, the T_K was estimated to be below 5 °C, indicating high water solubility independent of the alkyl chain length. The T_K of $2C_n$(2-O-2) with the hydrophobic counterion $(CF_3SO_2)_2N^-$ (NTf_2) is 43 °C at 0.010 wt%,[30] whereas that of $2C_n$(2-O-2) with an aromatic carboxylate counterion is > 60 °C at 0.02 wt%.[45] This shows that the presence of fluorine or an aromatic ring in the counterion considerably lowers water solubility. In contrast, the glycinate counterion, which contains both a carboxylate ion and amino group, increases the water solubility of gemini surfactants.

Surface tension

Fig. 2 shows the variation in surface tension with surfactant concentration at 25 °C for $2C_n$(2-O-2) Gly and $2C_n$(2-O-2) Br (n = 10, 12, and 14). The error bars in Fig. 2 represent measurement uncertainties, which were evaluated based on repeated measurements. The surface tension of $2C_n$(2-O-2) Br exhibited the typical behavior: decreasing with increasing surfactant concentration, reaching a distinct breakpoint considered as the CMC, and then remaining constant. On the other hand, the surface tension of $2C_n$(2-O-2) Gly exhibited a unique behavior. Initially, it decreased with increasing surfactant concentration, reaching a considerably low minimum value. Subsequently, it increased with a further increase in concentration, after which it remained mostly constant. In general, when a surfactant solution contains impurities, the plot of surface tension versus concentration often shows a minimum at concentrations near the CMC.[46] However, the distinct minimum in the surface tension plot of $2C_n$(2-O-2) Gly cannot be attributed to impurities because the purity of the surfactant is high, as evidenced by ^{1}H NMR and elemental analyses (see Supplementary Information).

Fig. 3 shows the variation in electrical conductivity with the surfactant concentration at 25 °C for $2C_n$(2-O-2) Gly and $2C_n$(2-O-2) Br. The conductivity increased linearly with increasing concentration, followed by a gradual slope at a breakpoint, which corresponds to the beginning of micelle formation. The breakpoint was almost consistent with the minimum concentration observed in the surface tension plot, which corresponds to the CMC. To facilitate discussion of the unique interfacial adsorption behavior of $2C_n$(2-O-2) Gly, we subdivided

the surface tension versus concentration plot into three regions: (I) concentrations below the CMC; (II) concentrations

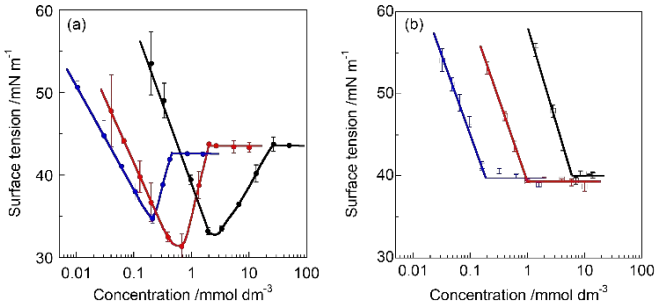

Fig. 2 Variation in surface tension with surfactant concentration for quaternary-ammonium-salt-based gemini surfactants. (a) $2C_{10}$(2-O-2) Gly (black solid circles), $2C_{12}$(2-O-2) Gly (red solid circles), and $2C_{14}$(2-O-2) Gly (blue solid circles). (b) $2C_{10}$(2-O-2) Br (black open squares), $2C_{12}$(2-O-2) Br (red open squares), and $2C_{14}$(2-O-2) Br (blue open squares).

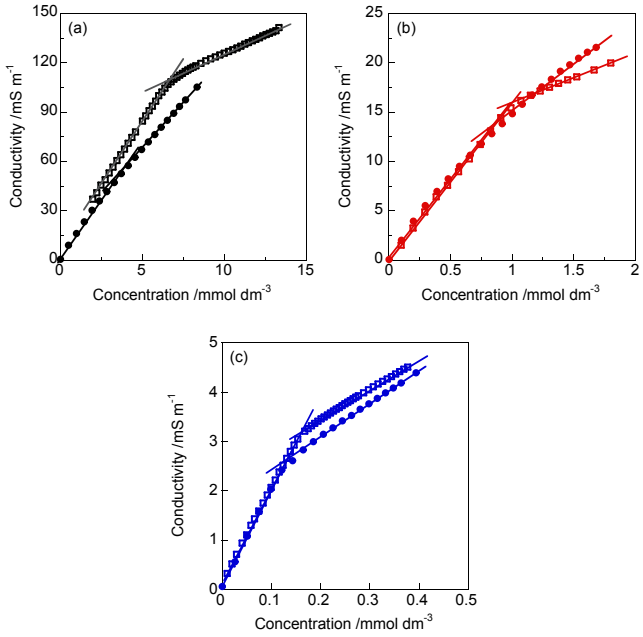

Fig. 3 Variation in conductivity with surfactant concentration for quaternary-ammonium-salt-based gemini surfactants. (a) $2C_{10}$(2-O-2) Gly (black solid circles) and $2C_{10}$(2-O-2) Br (black open squares). (b) $2C_{12}$(2-O-2) Gly (red solid circles) and $2C_{12}$(2-O-2) Br (red open squares). (c) $2C_{14}$(2-O-2) Gly (blue solid circles) and $2C_{14}$(2-O-2) Br (blue open squares). Error bars were omitted because of negligible measurement uncertainties.

from the CMC to the point where the surface tension becomes constant; and (III) concentrations at constant surface tension. The surface tension curve of $2C_n$(2-O-2) Br shows the absence of a minimum at the boundary between regions I and II, suggesting that the carboxylate ions and amino groups of $2C_n$(2-O-2) Gly contribute to specific interfacial adsorption. In region I, despite the bulky structure of the glycinate counterion, hydrogen bonding between the amino nitrogen of $2C_n$(2-O-2) Gly and hydrogen atoms of water, as well as between the carboxylate oxygen of $2C_n$(2-O-2) Gly and hydrogen atoms of either the amino group or water, is strong, leading to dense adsorption and self-orientation of the surfactant at the air/water interface. The increase in surface tension in region II may result from the saturation of the interface with surfactant molecules, causing micelle formation in solution. Consequently, surfactant molecules move from the interface to the bulk phase, decreasing the interfacial density and increasing the surface tension.

The minimum in the surface tension plot was also observed for $2C_n$(2-O-2) OH, where the counterion is a hydroxy ion (Fig. S1). Similar to the case of $2C_n$(2-O-2) Gly, this can be attributed to hydrogen bonding between the hydroxy groups and between the hydroxy group and water. We previously reported that alanine-based surfactants with a hydroxy counterion exhibit a distinct minimum in the surface tension plot at a concentration near the CMC, which is attributed to intermolecular hydrogen bonding between the hydroxy group and carboxylate ion.[47]

Table 1 lists the CMC, surface tension at the CMC (γ_{CMC}), surface excess concentration (Γ), occupied area per molecule (A), adsorption efficiency (pC_{20}), effectiveness of the adsorption and micellization processes (CMC/C_{20}), and absolute values of the standard free energies of surface adsorption ($|\Delta G^{o}ads|$) and micelle formation ($|\Delta G^{o}mic|$) determined from the surface tension curves and dissociation degree (α) obtained from electrical conductivity measurements. The CMCs of $2C_n$(2-O-2) Gly and $2C_n$(2-O-2) Br decreased with increasing alkyl chain length. The CMC of $2C_n$(2-O-2) Gly was lower than that of $2C_n$(2-O-2) Br, and the difference in CMC at the same alkyl chain length was more pronounced at shorter alkyl chain lengths. This may be due to the formation of hydrogen bonding between the glycinate of $2C_n$(2-O-2) Gly and other molecules, as described above, which renders the counterion more hydrophobic, resulting in a lower CMC. In general, the CMC decreases logarithmically as the number of carbons (n) in the alkyl chain of a homologous series increases.[19] The relationship can be expressed by the so-called Klevens equation log CMC = $A - Bn$, where A and B are constants specific to the homologous series under constant conditions of temperature, pressure, and other parameters. From the linear relationship between the logarithm of the CMC and alkyl chain length of $2C_n$(2-O-2) Gly and $2C_n$(2-O-2) Br (Fig. S2), the B values corresponding to the slope of the line were 0.32 and 0.41, respectively. The B value of $2C_n$(2-O-2) Br is in good agreement with the reported value of 0.4.[48–50] The smaller B value of $2C_n$(2-O-2) Gly compared with that of $2C_n$(2-O-2) Br indicates a smaller degree of decrease in the CMC relative to the alkyl chain length. This is because the glycinate counterion of $2C_n$(2-O-2) Gly is bulky, which makes micelle formation more difficult than that for gemini surfactants with smaller counterions. Thus, the B values of gemini surfactants depend on the counterion.

The γ_{CMC} values of $2C_n$(2-O-2) Gly were 30–35 mN m^{-1}, indicating the excellent ability of these surfactants to reduce surface tension. Their constant surface tension (γ_{const}) values in region III were higher, ranging from 42 to 44 mN m^{-1}. The γ_{CMC} values of $2C_n$(2-O-2) Gly were considerably smaller than those of $2C_n$(2-O-2) Br, whereas its γ_{const} values were slightly larger. This can be attributed to the hydrogen bonding between the glycinate counterion of $2C_n$(2-O-2) Gly and other molecules. This hydrogen bonding resulted in dense adsorption and efficient orientation of the surfactant at the air/water interface, significantly reducing the γ_{CMC}. However, the γ_{const} increased at concentrations above the CMC owing to the desorption

of the surfactant from the interface. The A values of $2C_n$(2-O-2) Gly were larger than those of $2C_n$(2-O-2) Br and increased with increasing alkyl chain length. This is because $2C_n$(2-O-2) Gly has a bulkier structure than $2C_n$(2-O-2) Br, which allows it to spread and adsorb at

Table 1 Krafft temperature (T_K), critical micelle concentration (CMC), surface tension at the CMC (γ_{CMC}), constant surface tension (γ_{const}), surface excess concentration (Γ), occupied area per molecule (A), dissociation degree (α), adsorption efficiency (pC_{20}), effectiveness of the surface adsorption and micellization processes (CMC/C_{20}), and standard free energies of surface adsorption (ΔG^{o}_{ads}) and micelle formation (ΔG^{o}_{mic}) for $2C_n$(2-O-2) Gly and $2C_n$(2-O-2) Br at 25 °C.

	T_K (°C)	CMC[a] (mmol dm^{-3})	CMC[b] (mmol dm^{-3})	γ_{CMC} (mN m^{-1})	γ_{const} (mN m^{-1})	$\Gamma \times 10^6$ (mol m^{-2})	A (nm^2)	α	pC_{20}	CMC/C_{20}	$\lvert\Delta G^{o}_{ads}\rvert$ (kJ mol^{-1})	$\lvert\Delta G^{o}_{mic}\rvert$ (kJ mol^{-1})
$2C_{10}$(2-O-2) Gly	< 5	2.44	2.34 ± 0.07	31.5 ± 0.1	43.7 ± 1.5	1.20 ± 0.20	1.38 ± 0.27	0.778	3.68 ± 0.16	11.3 ± 5.6	58.5 ± 6.4	25.0 ± 0.1
$2C_{12}$(2-O-2) Gly	< 5	0.526	0.581 ± 0.052	29.6 ± 1.0	43.5 ± 0.4	0.909 ± 0.133	1.83 ± 0.31	0.668	4.71 ± 0.27	29.9 ± 12.4	75.0 ± 8.9	28.4 ± 0.2
$2C_{14}$(2-O-2) Gly	< 5	0.128	0.208 ± 0.002	34.6 ± 0.8	42.3 ± 0.4	0.717 ± 0.019	2.32 ± 0.06	0.350	5.13 ± 0.11	28.0 ± 7.6	83.1 ± 2.6	31.0 ± 0.02
$2C_{10}$(2-O-2) Br	< 5	6.76	5.48 ± 0.18	40.0 ± 0.3	—	1.58 ± 0.04	1.05 ± 0.03	0.293	2.80 ± 0.02	3.5 ± 0.1	48.8 ± 0.7	28.5 ± 0.01
$2C_{12}$(2-O-2) Br	< 5	1.03	0.975 ± 0.053	39.4 ± 0.2	—	1.17 ± 0.01	1.42 ± 0.02	0.319	3.69 ± 0.04	4.8 ± 0.2	60.7 ± 0.6	32.9 ± 0.2
$2C_{14}$(2-O-2) Br	< 5	0.160	0.210 ± 0.003	39.7 ± 0.2	—	1.05 ± 0.07	1.58 ± 0.11	0.316	4.41 ± 0.06	5.4 ± 0.7	68.2 ± 2.4	37.5 ± 0.05

[a] Determined from conductivity measurements. [b] Determined from surface tension measurements.

the air/water interface. Furthermore, it may be oriented more efficiently because the carboxylate ion and amino group of glycinate can form hydrogen bonds. The decrease in surface tension of these gemini surfactants is consistent with the pC_{20} and $|\Delta G^{o}ads|$ values. The pC_{20} and $|\Delta G^{o}ads|$ values of $2C_n$(2-O-2) Gly were larger than those of $2C_n$(2-O-2) Br at the same alkyl chain length and increased with increasing alkyl chain length. On the other hand, the $|\Delta G^{o}mic|$ values of $2C_n$(2-O-2) Gly were smaller than those of $2C_n$(2-O-2) Br, but its CMC/C_{20} values were considerably larger. Thus, $2C_n$(2-O-2) Gly is less likely to aggregate in solution owing to the presence of the bulky glycinate counterion, in contrast to its behavior at the air/water interface. This observation is further supported by its α values obtained from the electrical conductivity measurements, which were larger than those of $2C_n$(2-O-2) Br. A similar behavior was reported for monomeric surfactants such as the dodecyl sulfate salt.[51]

Aggregation properties

We investigated the structure of the aggregates formed by $2C_n$(2-O-2) Gly (n = 10, 12, and 14) in D_2O using the SANS technique. Fig. 4 shows the SANS profiles of $2C_{10}$(2-O-2) Gly (50, 100, 150, 200, 250, 300, 400, and 500 mmol dm^{-3}), $2C_{12}$(2-O-2) Gly (50, 100, 150, 200, 250, and 300 mmol dm^{-3}) and $2C_{14}$(2-O-2) Gly (50, 100, 150, 200, and 250 mmol dm^{-3}), along with the best-fit theoretical scattering curves obtained using Eqs. (1)–(6). All SANS profiles showed a scattering vector (q) dependence of the scattering intensity $I(q)$, $I(q) \sim q^0$, in the low q range of 0.3–0.6 nm^{-1}. All profiles exhibited a peak in the range q = 0.6–2.0 nm^{-1}, which reflects the interference between scattering particles due to the repulsion between micelles. Flexible one-dimensional objects are known to elongate beyond the distance to their first neighbor; thus, $q_m \propto \varphi^{1/2}$, where q_m is the q value of the peak and φ is the volume fraction of surfactant molecules.[52] In other words, the formation of rod- or worm-like micelles is likely. The solution of colloidal particles interacting at distances larger than their own size, such as spherical micelles, is characterized by $q_m \propto \varphi^{1/3}$. [53] Fig. S3 shows the variation in q_m with φ for $2C_n$(2-O-2) Gly. The relationship between q_m and φ followed a straight line with a slope of 1/3. This indicates that $2C_n$(2-O-2) Gly forms spherical micelles over a wide range of concentration, independent of the alkyl chain length.

The $I(q)$ of the profile of $2C_n$(2-O-2) Gly increased with increasing concentration. Because $2C_n$(2-O-2) Gly forms spherical micelles at $q > 1/R_g$, the scattering reflects the shape of individual particles, interfaces between particles, and heterogeneity of the particles. By dividing $I(q)$ by the φ of $2C_n$(2-O-2) Gly, the scattering in the high q region of the profile at all concentrations becomes equal to that of the isolated system, unaffected by interparticle interference and independent of φ.

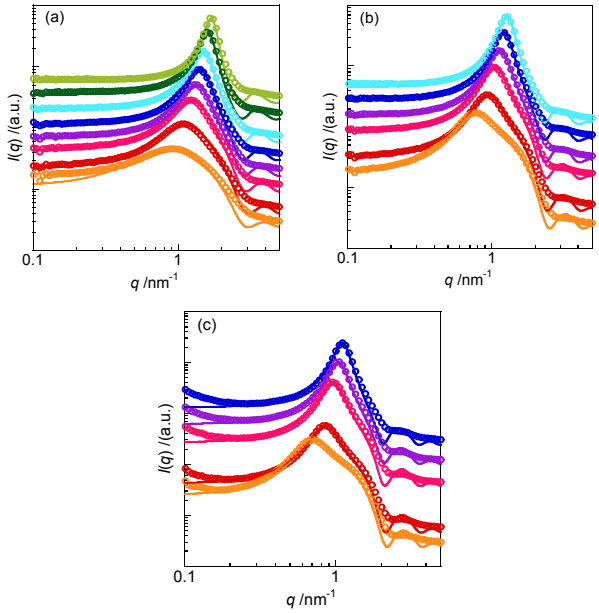

Fig. 4 Concentration dependence of the SANS profiles (open circles) of $2C_n$(2-O-2) Gly and fitted scattering curves. (a) $2C_{10}$(2-O-2) Gly, (b) $2C_{12}$(2-O-2) Gly, and (c) $2C_{14}$(2-O-2)

Gly at concentrations of 50 (orange), 100 (red), 150 (pink), 200 (violet), 250 (blue), 300 (royal blue), 400 (green), and 500 mmol dm^{-3} (pea green).

Fig. S4 shows the scattering profile of 2C$_n$(2-O-2) Gly normalized by φ. The q_m peak shifted toward higher q values with increasing concentration for both alkyl chain lengths. This behavior of the q_m peak, which reflects micelle interaction, was also observed in the SANS profiles of other quaternary-ammonium-salt-based gemini surfactants.[14,39,54] In the low q region, the decrease in $I(q)$ increased with increasing 2C$_n$(2-O-2) Gly concentration, regardless of the alkyl chain length. This is because as φ increases, the compressibility of the osmotic pressure in the particle dispersion system decreases, suppressing particle concentration fluctuations. Consequently, $I(q = 0)$ decreased (negative interparticle interference effect), and a broad scattering peak with a scattering maximum I_m at q_m corresponding to the mean interparticle distance d was observed.

The SANS profiles of 2C$_n$(2-O-2) Gly were fitted using an overall ellipsoid model. Table 2 lists the radii of the major and minor axes (R_1 and R_2) and the axial ratio (v) for the ellipsoidal micelles formed by 2C$_n$(2-O-2) Gly. Fig. 5 shows the relationship between R_1, R_2, v, and the surfactant concentration of the ellipsoidal micelles, which were obtained through model-based analysis. An increase in $I(q)$ was observed in the $q < 0.2$ nm^{-1} region of the SANS profile of 2C$_{14}$(2-O-2) Gly, which indicates the possible aggregation of the micelles. The fully extended lengths of the alkyl chain (l_c), calculated using the Tanford equation,[55] were 1.29, 1.55, and 1.80 nm for n = 10, 12, and 14, respectively (dotted lines in Fig. 5). Except in the case of 50 mmol dm^{-3} 2C$_{10}$(2-O-2) Gly, the R_2 values of the ellipsoidal micelles were greater than the corresponding l_c values. This difference can be attributed to the size of the quaternary ammonium salt, as the overall micelle radius includes both the

Table 2 Structural parameters obtained from model-fitting analysis of the SANS profiles of 2C$_n$(2-O-2) Gly.

	Concentration (mmol dm^{-3})	R_1[a] (nm)	R_2[b] (nm)	v[c]	$\Delta\rho$[d] (10^{10} cm^{-2})	N_{agg}[e]
2C$_{10}$(2-O-2) Gly	50	1.353	1.325	1.02	–4.67	16
	100	1.517	1.443	1.05	–4.82	20
	150	1.579	1.496	1.06	–4.94	21
	200	1.657	1.510	1.10	–4.95	22
	250	1.689	1.534	1.10	–4.88	23
	300	1.718	1.540	1.12	–4.91	23
	400	1.800	1.550	1.16	–4.90	24
	500	1.879	1.566	1.20	–4.85	25
2C$_{12}$(2-O-2) Gly	50	1.779	1.779	1.00	–5.22	22
	100	1.904	1.813	1.05	–5.22	23
	150	1.993	1.829	1.09	–5.20	24
	200	2.025	1.841	1.10	–5.18	25
	250	2.079	1.856	1.12	–5.17	26
	300	2.116	1.856	1.14	–5.15	26
2C$_{14}$(2-O-2) Gly	50	2.073	2.030	1.02	–5.32	23
	100	2.153	2.060	1.05	–5.30	24
	150	2.202	2.079	1.06	–5.27	24
	200	2.272	2.080	1.09	–5.26	25
	250	2.337	2.087	1.12	–5.24	25

[a] Radius of the major axis of the ellipsoidal micelle. [b] Radius of the minor axis of the ellipsoidal micelle. [c] Axial ratio. [d] Scattering contrast. [e] Aggregation number.

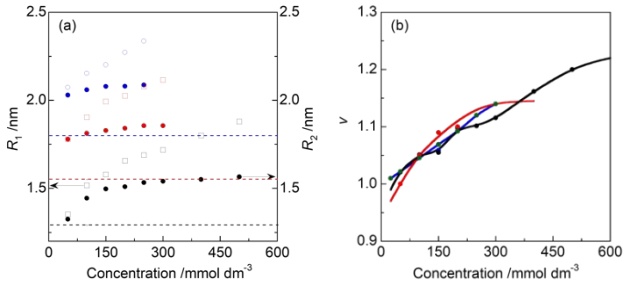

Fig. 5 Relationships between the (a) radii of the major and minor axes of micelles (R_1 and R_2) and (b) axial ratio (v) and the concentration of 2C$_n$(2-O-2) Gly, where n = 10 (black), 12 (red), 14 (blue). The dotted lines show the fully extended lengths of the alkyl chain.

alkyl chains and hydrophilic groups. The micelle radius at 50 mmol dm^{-3} 2C$_{10}$(2-O-2) Gly was almost the same as the l_c value. This suggests that the micelles formed at low concentrations are unstable owing to the short chain length. The R_2 values of the ellipsoidal micelles increased with increasing concentration and were nearly constant at concentrations above 150 mmol dm^{-3}. In contrast, the R_1 values continuously increased as the surfactant concentration increased, resulting in an increase in v. Thus, as the 2C$_n$(2-O-2) Gly concentration increased, the micelles transitioned from a spherical to an ellipsoidal structure.

The aggregation number (N_{agg}) of 2C$_n$(2-O-2) Gly was calculated by dividing the surface area of the ellipsoidal micelle in aqueous solution by the occupied area per surfactant molecule (A). Here, the molecular occupied area in the micelle is assumed to be equivalent to that at the air/water interface. The calculated N_{agg} values are summarized in Table 2. For 2C$_{10}$(2-O-2) Gly, N_{agg} varied between 16 and 25 in the concentration range of 50–500 mmol dm^{-3}. Similarly, N_{agg} ranged from 22 to 26 at 50–300 mmol dm^{-3} for 2C$_{12}$(2-O-2) Gly and from 23 to 25 at 50–250 mmol dm^{-3} for 2C$_{14}$(2-O-2) Gly. In all cases, N_{agg} increased slightly with increasing surfactant concentration. As discussed earlier, this trend is attributed to the elongation of both the major and minor axes of the ellipsoidal micelle as the concentration increases, leading to micelle growth and a corresponding increase in N_{agg}. Furthermore, N_{agg} increased as the alkyl chain length of 2C$_n$(2-O-2) Gly increased from n = 10 to 12 but remained nearly constant at n = 14. This suggests that while increasing the alkyl chain length up to n = 12 promotes micelle formation, a saturation point is reached beyond this length. A possible explanation for this behavior is steric limitation within the micellar core. As the alkyl chain length increases, the hydrophobic core volume increases. This imposes spatial constraints on the arrangement of surfactant molecules, thereby restricting a further increase in N_{agg}. Hydration effects at the micellar interface may also contribute to this saturation. Longer alkyl chains increase interfacial rigidity, reducing the likelihood of additional surfactant molecules incorporating into the micelle. Consequently, N_{agg} becomes less sensitive to a further increase in alkyl chain length beyond n = 12. These findings align with the general trend in micelle formation, in

which N_{agg} does not increase indefinitely with the alkyl chain length but instead plateaus owing to steric, structural, and interfacial interactions.

A notable difference was observed between the N_{agg} values of $2C_{12}$(2-O-2) Gly and $2C_{12}$(2-O-2) Br with a bromide counterion. At 50 mmol dm^{-3}, the N_{agg} of $2C_{12}$(2-O-2) Br was 47, which is nearly twice that of $2C_{12}$(2-O-2) Gly. This substantial difference can be attributed to the structural and hydration properties of the counterions. Glycinate, an amino-acid-derived counterion, contains carboxylate ($–COO^-$) and amine ($–NH_2$) functional groups, which make it bulkier and more highly hydrated than bromide. The extensive hydration shell around glycinate weakens electrostatic shielding between surfactant head groups, increasing repulsion and preventing compact molecular packing within the micelle. The bulkiness of glycinate also introduces additional steric hindrance at the micellar interface, further impeding the close packing of surfactant molecules. In contrast, bromide, being a small monovalent counterion with relatively weak hydration, effectively shields the electrostatic repulsion between head groups, facilitating the formation of micelles with a higher N_{agg}. Consequently, the N_{agg} of $2C_{12}$(2-O-2) Br was significantly higher than that of $2C_{12}$(2-O-2) Gly. These findings are consistent with the general trend that bulky and highly hydrated counterions reduce aggregation, whereas small and weakly hydrated counterions promote compact micelle formation.

The lower N_{agg} of $2C_{12}$(2-O-2) Gly compared with that of $2C_{12}$(2-O-2) Br can also be interpreted in terms of the dissociation degree (α), as determined from the conductivity measurements. When glycinate serves as the counterion, α approaches 1, indicating that the counterion remains largely dissociated from the micellar surface and dispersed in solution. This reduces electrostatic shielding between surfactant head groups, thereby increasing repulsion. Thus, it is more difficult for surfactant molecules to assemble densely, ultimately leading to a lower N_{agg}. Conversely, when bromide is the counterion, α is significantly lower, indicating its strong binding to the micellar surface. This enhances electrostatic shielding, thereby reducing repulsion between the head groups. Consequently, a greater number of surfactant molecules are incorporated into the micelle, resulting in a higher N_{agg}.

These findings indicate that differences in counterion binding, as reflected in the dissociation degree, significantly impact micelle aggregation behavior. The interplay of steric effects, hydration, and electrostatic shielding governs the aggregation number, demonstrating that micelle formation is not solely dictated by the alkyl chain length but also strongly influenced by counterion properties.

Conclusions

In this study, we synthesized quaternary-ammonium-salt-based gemini surfactants with glycinate as the counterion (n = 10, 12, 14) and investigated their adsorption and aggregation properties by measuring the conductivity, surface tension, and SANS. The surface tension of $2C_n$(2-O-2) Gly decreased with increasing surfactant concentration, exhibiting a distinct minimum at the CMC, a unique interfacial adsorption behavior not typically observed with conventional surfactants. The surface tension of $2C_n$(2-O-2) Gly ranged from 29.6 to 34.6 mN m^{-1}, which was lower than that of $2C_n$(2-O-2) Br. This lower surface tension can be attributed to enhanced hydrogen bonding between the amino nitrogen of the counterion and hydrogen atoms of water, as well as between the carboxylate oxygen of the counterion and hydrogen atoms of either the amino group or water. Therefore, gemini surfactants with a glycinate counterion adsorb and orient themselves efficiently at the air/water interface. In an aqueous solution, $2C_n$(2-O-2) Gly formed ellipsoidal micelles with the major axis radius ranging from 1.353 to 2.337 nm and the minor axis radius ranging from 1.325 to 2.087 nm. This suggests that the size and shape of the micelles are concentration dependent; specifically, the axial ratio of the micelles increased, and their structure transitioned from spherical to ellipsoidal with increasing concentration.

Although many quaternary-ammonium-salt-based gemini surfactants have been studied, there have been no reports on those with an amino acid as the counterion. This study highlights the influence of the counterion structure on surfactant properties. In the future, we aim to synthesize gemini surfactants with various amino acids as counterions and investigate the effect of structural variation on their physicochemical properties, particularly adsorption and aggregation behaviors.

Author Contributions

Shan Wang: investigation, writing – original draft. Hiroki Iwase: validation, supervision. Shin-ichi Takata: supervision. Risa Kawai: investigation. Shiho Yada: investigation, resources, validation. Tomokazu Yoshimura: conceptualization, supervision, writing – review and editing.

Conflicts of interest

The authors declare that they have no competing financial interests or personal relationships that could have influenced the work reported in this study.

Data availability

The data supporting this article have been included as part of the Supplementary Information.

Acknowledgements

This work was supported by the Support for Pioneering Research Initiated by the Next Generation (SPRING) program of the Japan Science and Technology Agency (Grant No. JPMJSP2115). SANS experiments were performed at the Materials and Life Science Experimental Facility of J-PARC under a user program (Proposal No. 2022I0015). The authors thank Editage (www.editage.jp) for English language editing.

References

1 R. Zana and J. Xia, *Gemini Surfactants: Synthesis, Interfacial and Solution-Phase Behavior, and Applications,* CRC Press, Boca Raton, 2003.

2 M. J. Rosen and J. T. Kunjappu, *Surfactants and Interfacial Phenomena,* John Wiley & Sons, New York, 2012.

3 R. Zana, *J. Colloid Interface Sci.*, 2002, **248**, 203.

4 Th. Dam, J. B. F. N. Engberts, J. Karthäuser, S. Karaborni and N. M. van Os, *Colloids Surf. A*, 1996, **118**, 41.

5 T. Yoshimura, M. Bong, K. Matsuoka, C. Honda and K. Endo, *J. Colloid Interface Sci.*, 2009, **339**, 230.

6 K. Sakai, M. Kaji, Y. Takamatsu, K. Tsuchiya, K. Torigoe, K. Tsubone, T. Yoshimura, K. Esumi, H. Sakai and M. Abe, *Colloids Surf. A*, 2009, **333**, 26.

7 P. X. Li, C. C. Dong, R. K. Thomas and Y. L. Wang, *Langmuir*, 2011, **27**, 656.

8 T. Yoshimura, T. Ichinokawa, M. Kaji and K. Esumi, *Colloids Surf. A,* 2006, **273**, 208.

9 K. Nyuta, T. Yoshimura and K. Esumi, *J. Colloid Interface Sci.*, 2006, **301**, 267.

10 T. Yoshimura and K. Nyuta, *J. Oleo Sci.,* 2017, **66**, 1139.

11 K. Nyuta, T. Yoshimura, K. Tsuchiya, H. Sakai, M. Abe and H. Iwase, *J. Colloid Interface Sci.*, 2012, **370**, 80.

12 T. Morita, S. Yada and T. Yoshimura, *Langmuir*, 2022, **38**, 156.

13 X. Pei, J. Zhao and E. Li, *Colloids Surf. A*, 2013, **420**, 59.

14 V. Sharma, M. Borse, V. K. Aswal, N. K. Pokhriyal, J. V. Joshi, P. S. Goyal and S. Devi, *J. Colloid Interface Sci.*, 2004, **277**, 450.

15 T. Yoshimura, A. Sakato and K. Esumi, *J. Oleo Sci.*, 2013, **62**, 579.

16 P. H. Elworthy and K. J. Mysels, *J. Colloid Interface Sci.*, 1966, **21**, 331.

17 K. J. Mysels and L. H. Princen, *J. Phys. Chem.*, 1959, **63**, 1696.

18 P. Mukerjee, *Adv. Colloid Interface Sci.*, 1967, **1**, 242.

19 H. B. Klevens, *J. Phys. Colloid Chem.*, 1948, **52**, 130.

20 H. W. Hoyer and A. Marmo, *J. Phys. Chem.*, 1961, **65**, 1807.

21 M. J. Rosen, M. Dahanayake and A. W. Cohen, *Colloids Surf.*, 1982, **5**, 159.

22 I. Mandru, *J. Colloid Interface Sci.*, 1972, **41**, 430.

23 A. Packter and M. Donbrow, *J. Pharm. Pharmacol.*, 1963, **15**, 317.

24 I. D. Robb and R. Smith, *J. Chem. Soc. Faraday Trans. 1*, 1974, **70**, 287.

25 K. Shinoda, M. Hato and T. Hayashi, *J. Phys. Chem.*, 1972, **76**, 909.

26 R. Oda, I. Huc and S. J. Candau, *Angew. Chem. Int. Ed.*, 1998, **37**, 2689.

27 R. Oda, I. Huc, M. Schmutz, S. J. Candau and F. C. MacKintosh, *Nature*, 1999, **399,** 566.

28 N. Jiang, P. Li, Y. Wang, J. Wang, H. Yan and R. K. Thomas, *J. Phys. Chem. B*, 2004, **108**, 15385.

29 R. Kawai, S. Yada and T. Yoshimura, *ACS Omega*, 2019, **4**, 14242.

30 R. Kawai, M. Niki, S. Yada and T. Yoshimura, *Colloids Surf. A*, 2020, **603**, 125218.

31 M. Rojas, J. G. Santos, E. Orth, R. Figueroa and P. Pavez, *J. Mol. Liq.*, 2020, **310**, 113206.

32 E. Alopina, Y. Dobryakov, E. Safonova, N. Smirnova, E. Kolobova and L. Kartsova, *Colloids Surf. A*, 2018, **544**, 137.

33 X.-J. Yang, P. Zhang, W. Lv, T. Zhou, P. Li and M. Zhao, *J. Surfactants Deterg.*, 2019, **22**, 515.

34 S. Takata, J. Suzuki, T. Shinohara, T. Oku, T. Tominaga, K. Ohishi, H. Iwase, T. Nakatani, Y. Inamura, T. Ito, K. Suzuya, K. Aizawa, M. Arai, T. Otomo and M. Sugiyama, *J. Phys. Soc. Jpn.*, 2015, **8**, 036020.

35 F. Zhang, J. Ilavsky, G. G. Long, J. P. G. Quintana, A. J. Allen and P. R. Jemian, *Metall. Mater. Trans. A*, 2010, **41**, 1151.

36 S. Prévost, L. Wattebled, A. Laschewsky and M. Gradzielski, *Langmuir*, 2011, **27**, 582.

37 J. S. Pedersen, *Adv. Colloid Interface Sci.*, 1997, **70**, 171.

38 J. B. Hayter and J. Penfold, *Colloid Polym. Sci.*, 1983, **261**, 1022.

39 H. Hirata, N. Hattori, M. Ishida, H. Okabayashi, M. Frusaka, and R. Zana, *J. Phys. Chem.*, 1995, **99**, 17778.

40 M. Kakitani, T. Imae and M. Furusaka, *J. Phys. Chem.*, 1995, **99**, 16018.

41 L. M. Bergström, A. Tehrani-Bagha and G. Nagy, *Langmuir*, 2015, **31**, 4644.

42 J. B. Hayter and J. Penfold, *Mol. Phys.*, 1981, **42**, 109.

43 M. Kotlarchyk and S. H. Chen, *J. Chem. Phys.*, 1983, **79**, 2461.

44 J.-P. Hansen and J. B. Hayter, *Mol. Phys.*, 1982, **46**, 651.

45 S. Manet, Y. Karpichev, D. Bassani, R. Kiagus-Ahmad and R. Oda, *Langmuir*, 2010, **26**, 10645.

46 C. M. Persson, P. M. Claesson and K. Lunkenheimer, *J. Colloid Interface Sci.*, 2002, **251,** 182.

47 S. Yada, M. Wakizaka, H. Shimosegawa, H. Fujita, M. Yamada, Y. Matsue and T. Yoshimura, *Colloids Surf. A*, 2021, **611**, 125757.

48 R. Zana and H. Lévy, *Colloids Surf. A*, 1997, **127,** 229.

49 R. Zana, M. Benrraou and R. Rueff, *Langmuir*, 1991, **7**, 1072.

50 S. Zhang, J. Yu, J. Wu, W. Tong, Q. Lei and W. Fang, *J. Chem. Eng. Data*, 2014, **59,** 2891.

51 K. S. Rao, T. Singh, T. J. Trivedi and A. Kumar, *J. Phys. Chem. B*, 2011, **115**, 13847.

52 L. Cannavacciuolo, J. S. Pedersen and P. Schurtenberger, *Langmuir*, 2002, **18**, 2922.

53 M. In, B. Bendjeriou, L. Noirez and I. Grillo, *Langmuir*, 2010, **26**, 10411.

54 S. Chavda, K. Kuperkar and P. Bahadur, *J. Chem. Eng. Data*, 2011, **56**, 2647.

55 S. Krimm, *J. Polym. Sci. Polym. Lett. Ed.*, 1980, **18**, 687.

Data Availability Statement:

The data supporting this article have been included as part of the Supplementary Information.